Engineering 4 (2018) 311–320

Contents lists available at ScienceDirect

Engineering

journal homepage: www.elsevier.com/locate/eng

Research
Green Industrial Processes—Perspective

Surface-Driven High-Pressure Processing

Keith E. Gubbins [a,*], Kai Gu [b], Liangliang Huang [c,*], Yun Long [d], J. Matthew Mansell [a], Erik E. Santiso [a,*], Kaihang Shi [a], Małgorzata Śliwińska-Bartkowiak [e], Deepti Srivastava [a]

[a] Department of Chemical and Biomolecular Engineering, North Carolina State University, Raleigh, NC 27695-7905, USA
[b] Department of Chemistry, Zhejiang University, Hangzhou 310027, China
[c] School of Chemical, Biological and Materials Engineering, The University of Oklahoma, Norman, OK 73019, USA
[d] Department of Chemical and Biomolecular Engineering, National University of Singapore, Singapore 117585, Singapore
[e] Faculty of Physics, Adam Mickiewicz University in Poznań, Poznań 61-614, Poland

ARTICLE INFO

Article history:
Received 17 December 2017
Revised 6 February 2018
Accepted 10 May 2018
Available online 22 May 2018

Keywords:
Confinement
High pressure
High pressure phase
High pressure reaction
High pressure manufacture
High pressure chemical processing

ABSTRACT

The application of high pressure favors many chemical processes, providing higher yields or improved rates in chemical reactions and improved solvent power in separation processes, and allowing activation barriers to be overcome through the increase in molecular energy and molecular collision rates. High pressures—up to millions of bars using diamond anvil cells—can be achieved in the laboratory, and lead to many new routes for chemical synthesis and the synthesis of new materials with desirable thermodynamic, transport, and electronic properties. On the industrial scale, however, high-pressure processing is currently limited by the cost of compression and by materials limitations, so that few industrial processes are carried out at pressures above 25 MPa. An alternative approach to high-pressure processing is proposed here, in which very high local pressures are generated using the surface-driven interactions from a solid substrate. Recent experiments and molecular simulations show that such interactions can lead to local pressures as high as tens of thousands of bars (1 bar = 1×10^5 Pa), and even millions of bars in some cases. Since the active high-pressure processing zone is inhomogeneous, the pressure is different in different directions. In many cases, it is the pressure in the direction parallel to the surface of the substrate (the tangential pressure) that is most greatly enhanced. This pressure is exerted on the molecules to be processed, but not on the solid substrate or the containing vessel. Current knowledge of such pressure enhancement is reviewed, and the possibility of an alternative route to high-pressure processing based on surface-driven forces is discussed. Such surface-driven high-pressure processing would have the advantage of achieving much higher pressures than are possible with traditional bulk-phase processing, since it eliminates the need for mechanical compression. Moreover, no increased pressure is exerted on the containing vessel for the process, thus eliminating concerns about materials failure.

1. A new green route to high-pressure manufacturing

Pressure is a fundamental thermodynamic variable that has the potential to control and enhance the manufacture of chemicals and solid materials with a wide range of desired properties. High pressures are necessary in many manufacturing processes in the chemical, oil and gas, food, pharmaceutical, agrichemicals, and materials industries. Such compression is often required to achieve satisfactory yields and rates in chemical reactors and solvent power in separations, and for the synthesis of novel, high-pressure materials. Familiar examples are the Haber process to produce ammonia (typically 15–25 MPa); the manufacture of methanol from syngas (usually 5–10 MPa); high-pressure hydrogenation, carbonylation, and amination reactions (to 1.5 MPa); the synthesis of pharmaceuticals; and supercritical gas extraction and reaction (7–40 MPa). In conventional processing, these pressures are achieved through the compression of a bulk phase. However, such compression is expensive, because of both the thermodynamic work required and the need to develop multistage pumps that can withstand these pressures. As a result, high-pressure industrial processes seldom exceed a pressure of about 25 MPa (250 bar), largely due to materials limitations. Since the pressure exerted on the walls of

* Corresponding authors.
E-mail addresses: keg@ncsu.edu (K.E. Gubbins), hll@ou.edu (L. Huang), eesantis@ncsu.edu (E.E. Santiso).

https://doi.org/10.1016/j.eng.2018.05.004

the containing vessel is the same as that felt by the molecules to be processed, much higher pressures lead to equipment failure. Higher pressures (up to millions of bars using diamond anvil cells) can be studied in the laboratory, which makes possible the synthesis of many chemicals and materials using novel reaction mechanisms [1]. However, industrial-scale production using conventional approaches to compression is not practical.

In traditional high-pressure processing, the fluid is uniform and the pressure is a scalar constant throughout, equal in all directions. The pressure, $P = P_K + P_C$, consists of a kinetic contribution due to molecular motion ($P_K = RT/V$, the ideal gas value) and a configurational part, P_C, due to intermolecular forces and the action of any external fields. Unless the temperature is very high, the configurational contribution is usually the dominant one (typically 80%–90% of the total pressure at condensed matter temperatures). This suggests that it must be possible to create high pressures through the application of an external field that exerts significant forces on the molecules. Such a field would create inhomogeneity in the fluid, so that the pressure would then be a second-order tensor, dependent on both the direction of the force and the direction of the surface that it acts on. In the high-pressure processing proposed here, the interaction field exerted by the surface of a solid substrate on an adsorbed phase that wets the substrate is of particular interest.

There is much recent experimental evidence that the molecules in a fluid or solid film adsorbed on a solid substrate can experience strong compression in the lateral direction parallel to the solid surface, due to the strong attractive forces provided by the substrate. This compression is a surface-driven high-pressure effect. Such compression has been observed by direct *in situ* experiments; examples include measurements of the area of substrate surface occupied per molecule [2–5], X-ray diffraction (XRD) [6], low-energy electron diffraction [7–9], microcalorimetry measurements [10], atomic force microscopy, and Raman spectroscopy [11–14]. Most of these works reported compression corresponding to pressures ranging from 1 to 10 GPa on the adsorbate molecules near the surface of the substrate. Compression in the adsorbed surface layers has also been observed in molecular simulations [15–28]. In the simulations, the pressure components normal and parallel (i.e., tangential pressure) to the substrate surface can be measured separately. Even for small adsorbate molecules with only simple van der Waals forces (e.g., noble gases, nitrogen, and methane), the tangential pressure is found to be greatly enhanced over the bulk-phase pressure, provided that the adsorbate wets the solid surface; the value depends on the nature of the substrate and the distance from the solid wall. For carbon substrates, these pressures often range from 0.5 to 8 GPa when the bulk phase in equilibrium with the adsorbed layer is at 0.1 MPa pressure—an enhancement of four or five orders of magnitude. It should be noted that these high tangential pressures are parallel to the surface, and exert no force on the wall itself. The normal pressure does exert force on the wall, but is much smaller, and can be either positive or negative [21]. Such compression is particularly evident for solid substrates with a high surface atomic density [28], such as carbons, as shown in Fig. 1.

These recent results suggest that it should be possible to design high-pressure nano-reactors to synthesize chemicals and materials that require pressures much greater than those that can be used in conventional manufacturing processes. These high pressures occur locally near the substrate surface. Although the high-pressure reactor region may extend over distances of only a few nanometers from the surface in the case of simple van der Waals forces (larger if electrostatic forces are also present), the total reaction volume can be relatively large since activated carbons typically have surface areas of 1000–2000 $m^2 \cdot g^{-1}$ or more (see discussion in Section 6). Further research is needed to provide sufficient fundamental understanding of these surface-driven high-pressure effects to guide the design of such transformational manufacturing methods.

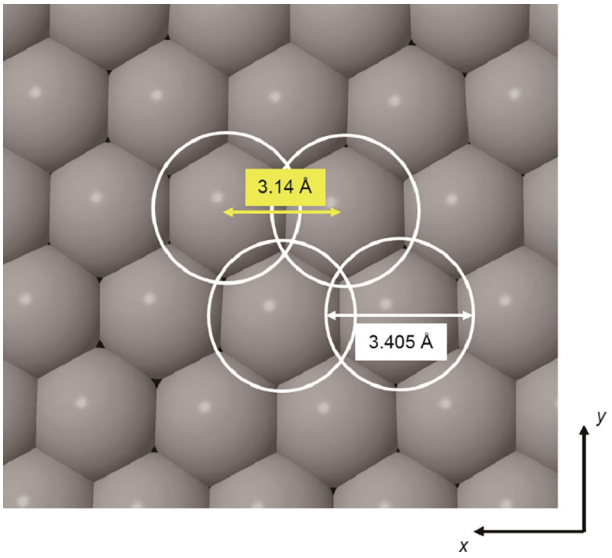

Fig. 1. Top view of a monolayer of Lennard–Jones (LJ) argon (Ar) atoms adsorbed on a graphite surface (not shown) lying in the *xy* plane, from molecular simulation, showing strong compression in the plane parallel to the surface. Neighboring molecules (gray color) are separated by 3.14 Å, much less than the separation (3.405 Å) when the pair force between two neighboring molecules is zero and no compression occurs (white circles) [28].

2. The local pressure in thin adsorbed films

Pressure is the force per unit area that acts on a surface element. In a bulk homogeneous isotropic phase, pressure is a scalar and is the same in all directions and all positions. However, if the phase is inhomogeneous, for example due to the presence of a solid substrate, the forces—and hence the pressure—are different in different directions; the pressure also depends on the direction of the surface on which it acts. The pressure is thus a second-order tensor, $\boldsymbol{P}$, having nine components in general; the component $P_{\alpha\beta}$ is the force per unit area in the β direction acting on a surface pointing in the α direction. For substrate surfaces of simple geometry, such as planar, cylindrical, or spherical surfaces, the off-diagonal elements of the pressure tensor (e.g., P_{xy}, the pressure in the *y* direction acting on a surface pointing in the *x* direction) vanish, provided that the system is not under strain, leaving only three non-vanishing diagonal elements. Thus, for a planar substrate surface or a slit pore (Fig. 2(a)), the pressure tensor is as follows:

$$\boldsymbol{P} = \begin{bmatrix} P_{xx} & P_{xy} & P_{xz} \\ P_{yx} & P_{yy} & P_{yz} \\ P_{zx} & P_{zy} & P_{zz} \end{bmatrix} = \begin{bmatrix} P_T & 0 & 0 \\ 0 & P_T & 0 \\ 0 & 0 & P_N \end{bmatrix} \quad (1)$$

where $P_T = P_{xx} = P_{yy}$ is the tangential pressure parallel to the substrate surface (the *xx* and *yy* components are equal by symmetry) and $P_N = P_{zz}$ is the pressure normal to the substrate surface.

The condition of hydrostatic equilibrium (also known as mechanical equilibrium) states that once the system has reached equilibrium, there is no net transfer of momentum across the interface between the solid substrate and the adsorbed phase. This leads to the following condition [29,30]:

$$\nabla \cdot \boldsymbol{P} = -\rho(r)\nabla v(r) \quad (2)$$

where $\rho(r)$ is the density of molecules (number per unit volume) at position *r*, and v is the external field acting at *r*. In the cases to be considered here, the only external field is gravity, which is negligible compared with the other forces present, so Eq. (2) can be written as follows:

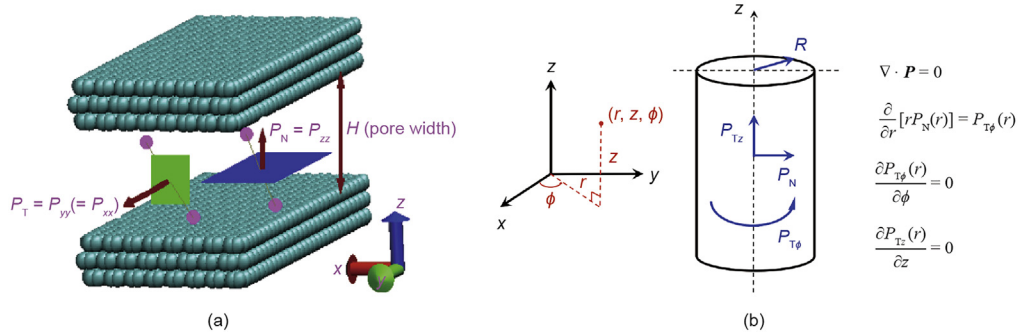

Fig. 2. (a) A slit-shaped carbon pore with three graphene layers in each wall, showing the normal, P_N, and tangential, P_T, pressures, and the surfaces they act on; (b) a cylindrical pore, showing the normal pressure, the two tangential pressures, and the equations of hydrostatic equilibrium.

$$\nabla \cdot \boldsymbol{P} = 0 \tag{3}$$

Eq. (3) provides three conditions on the components of the pressure. For the planar surface, assuming the surface to lie in the xy plane, with z normal to the surface, these conditions are that P_T is independent of both x and y (as expected from symmetry), while the normal pressure obeys the following:

$$\frac{dP_N}{dz} = 0 \tag{4}$$

Thus, the normal pressure is a constant for a given system, independent of the distance z from the surface of the substrate.

For a cylindrical interface, such as that of a cylindrical pore (Fig. 2(b)), the pressure tensor has three diagonal components: one normal to the pore wall, $P_N = P_{rr}$, and two parallel to the pore wall (the tangential components), $P_{Tz} = P_{zz}$ and $P_{T\phi} = P_{\phi\phi}$, where (r, z, ϕ) are the usual cylindrical polar coordinates. The equations resulting from the condition of hydrostatic equilibrium [31], given in Eq. (3), are shown in Fig. 2(b), and state that $P_{T\phi}$ and P_N are related by a first-order differential equation, while $P_{T\phi}$ is independent of the azimuthal angle, ϕ, and P_{Tz} is independent of the z coordinate. These latter two conditions are expected from symmetry. The first-order equation linking the normal pressure with the tangential pressure in the ϕ direction shows that there are actually only two independent pressures in cylindrical geometries, P_N and P_{Tz}.

3. Defining effective pressures in inhomogeneous phases

The conventional route to calculate the local pressure at a point r in the confined nano-phase is the so-called virial or mechanical route, in which one adds up the intermolecular forces acting on a surface element and divides by the area [29,30]; for pair additive potentials, this gives:

$$\boldsymbol{P}(\boldsymbol{r}) = \rho(\boldsymbol{r}) k_B T \mathbf{1} - \frac{1}{2}\left\langle \sum_{i \neq j} \frac{\partial u(ij)}{\partial \boldsymbol{r}_{ij}} \int_{C_{ij}} d\tilde{l}\, \delta\left(\boldsymbol{r} - \tilde{l}\right) \right\rangle \tag{5}$$

where $u(ij)$ is the pair potential between molecules i and j; C_{ij} is any arbitrary contour connecting the center of mass of molecule i, $\boldsymbol{r}_i$, to the center of mass of molecule j, $\boldsymbol{r}_j$, where $\boldsymbol{r}_{ij} = \boldsymbol{r}_j - \boldsymbol{r}_i$; k_B is the Boltzmann constant; T is temperature; $\mathbf{1}$ is the unit tensor; $\delta(\cdot)$ is the Dirac delta function; and <·> represents an ensemble average.

The first term on the right side of Eq. (5) is the ideal gas pressure, due to the kinetic energy of the molecules, while the second term on the right is the part of the pressure due to intermolecular forces. The pressure at a point r depends to some extent on the choice of contour C_{ij}, with that of Irving and Kirkwood (IK) being a common choice [32]. With the IK choice, the contour is a straight line joining the centers of molecules i and j; if this line intersects the element of area, the force contributes to the pressure. This non-uniqueness in the definition of the pressure at the nanoscale arises because the forces act between pairs (or triplets, etc.) of molecules, and there is no unique way to assign them to a specific point $\boldsymbol{r}$ in space. In calculating or measuring the pressure at the nanoscale, it is necessary to make an operational definition of $\boldsymbol{P}$, as was done by IK. We can regard such pressures as approximate effective pressures acting in a particular direction. When averaged over a suitably large distance, such local effective pressures should give well-defined unique values, independent of the operational definition used [29,30]. It should be noted that for the particular case of a planar surface, the normal pressure, P_N, is uniquely defined, even though the tangential pressure, P_T, is not. This follows from Eq. (5), which implies that P_N near the substrate surface has the same value as P_N far from the surface.

An alternative to the virial route is the "thermodynamic" route [25], which involves making small perturbations in the volume by an amount, ΔV; the length is perturbed in the α direction, keeping the other dimensions, L_β, constant. The pressure component $P_{\alpha\alpha}$ is as follows:

$$P^V_{\alpha\alpha} = -\left(\frac{\partial A}{\partial V}\right)_{N,T,L_{\beta\neq\alpha}} = \rho kT - \frac{kT}{\Delta V} \ln \left\langle \exp\left(\frac{-\Delta U}{kT}\right) \right\rangle_{N,T,L_{\beta\neq\alpha}} \tag{6}$$

where A is the Helmholtz energy, ΔU is the change in configurational energy due to the small volume perturbation, and the ensemble average is over the unperturbed system. The thermodynamic route offers an advantage over the virial route in that it is much easier to include three-body and higher effects in the force field using a thermodynamic route.

In addition to the virial and thermodynamic routes to $\boldsymbol{P}$, it is possible in some cases to use a third route to the pressure that is based on relating the structure of the adsorbed layers to two-dimensional (2D) or one-dimensional (1D) equations of state (EOSs), for slit pores and cylindrical pores, respectively. The advantage of this approach is that since the 2D and 1D systems are uniform, the pressure is well-defined, as it is in any three-dimensional (3D) uniform system. We have carried out initial tests of this route for the 2D case. The adsorbed layers near the wall are quasi-2D for slit pores (Fig. 3). During the simulation, the positions of the centers of the molecules in a given layer can be projected onto a strictly 2D plane, and the 2D density can be recorded; if an EOS is available for the 2D system, there will be a 2D pressure corresponding to the 2D density. This can be used to estimate the effective tangential pressure in the 3D slit pore system by dividing the 2D pressure by an appropriate length, such as the width of the density peak at half height [33]. The 2D density of these adsorbed layers is extremely high due to the compression—up to twice the density at the melting point. We have developed a highly accurate 2D EOS for the Lennard–Jones (LJ) system at these high densities

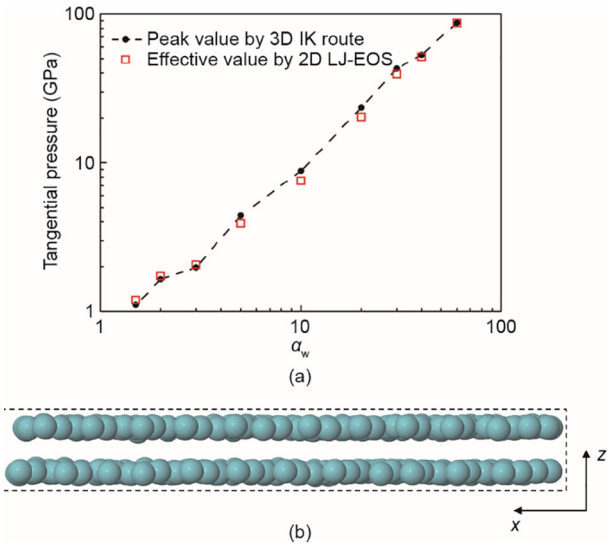

Fig. 3. (a) Comparison of the conventional 3D IK route and the 2D route to the tangential pressure for LJ Ar in a slit pore three molecular diameters in width at the boiling point of Ar (87.3 K, 1 bar (1 bar = 1×10^5 Pa) bulk pressure). Here, α_w is the microscopic wetting parameter (see Section 5 for definition). (b) Front view of two adsorbed layers in a slit pore three molecular diameters in width with $\alpha_w = 10$.

[33], and have used it to estimate the effective tangential pressures for a wide range of wetting parameters and pore widths. The resulting values of P_T from this "2D route" are in quite good agreement with those from the virial route, usually within 10%–20% (see Fig. 3(a)).

4. Experimental evidence for surface-driven high pressures

Thus far, experimental techniques to directly measure the pressure near the surface of a solid substrate have not been developed. It is possible to measure the normal pressure, P_N, acting on the substrate surface itself since it causes structural changes in the substrate material (e.g., changes to the pore width or interlayer spacing) that can be seen in XRD or neutron diffraction [21,34]. For planar surfaces, P_N is a constant that is independent of the distance z from the surface, but this is not the case for curved surfaces (see the conditions of hydrostatic equilibrium for cylindrical surfaces in Fig. 2(b)). However, compression of the molecules near the solid surface has been directly observed *in situ* in adsorption measurements of the area occupied by a molecule [2–5], microcalorimetry measurements [10], XRD [6], and low-energy electron diffraction [7–9]. These compression effects are most evident for solid substrates with a high surface atomic density, such as carbons.

In addition to these direct observations of molecular compression near a solid surface, there is much indirect evidence of high pressures in such surface films; experimental studies reveal high-pressure phases forming in nano-pores and high yields for chemical reactions carried out in nano-pores or on surfaces, even though such yields require very high pressures when the reactions are carried out in the bulk phase. Some examples of this type are discussed below.

4.1. High-pressure phases forming in nano-pores

High-pressure phases have often been observed to form in nano-porous materials even though the bulk phase in equilibrium with the pore phase is at ambient pressure or below [35–41]. For example, bulk-phase potassium iodide (KI) forms a B1 NaCl-type crystal structure ($Fm\bar{3}m$ space group) at ambient temperature and pressure, but undergoes a phase transition to a B2 CsCl-type crystal structure ($Pm\bar{3}m$ space group) at 1.9 GPa pressure [42]. However, Urita et al. [35] used high-resolution transmission electron microscopy (HRTEM) and synchrotron XRD to show that when confined within single-walled carbon nanotubes (SWCNTs) with an internal diameter of 2–5 nm, KI forms the high-pressure B2 phase, even though the bulk-phase KI that was in equilibrium with the pore was at a pressure below 0.1 MPa. A further example is the formation of methane hydrates in carbon nano-pores [43], a phase change that requires high pressure in the bulk phase. In addition to the formation of the hydrates at a low bulk pressure, confinement in carbon nano-pores leads to a dramatic increase in the kinetics of formation of the hydrate.

Solid–liquid transitions for organic compounds observed in surface force apparatus experiments often occur at temperatures well above their normal melting points, T_{mp}, suggesting high pressures. In these experiments, the organic nano-phase is confined between mica surfaces. For example, *n*-dodecane (T_{mp} = 263.4 K) freezes at 300 K, while cyclohexane (T_{mp} = 279 K) freezes at 296 K when confined between mica surfaces [37,39]. In the bulk phase, *n*-dodecane freezes at a pressure of ~1860 bar (1 bar = 1×10^5 Pa) at 300 K, while cyclohexane freezes at a pressure of ~440 bar. These high-pressure effects in confinement are consistent with molecular simulation studies, in which relatively small increases in the pressure of the bulk phase that is in equilibrium with the confined nano-phase cause large increases in the tangential pressure in the nano-pores [20,24,25].

4.2. Deformation of molecular structure in confined nano-phases

The discovery of 2D graphene has led to intense interest in 2D materials; about 1000 2D materials have now been synthesized or predicted to be possible, including 2D boron and other nitrides, 2D molybdenum sulfide, and 2D transition metal dichalcogenides [44,45]. Very recently, studies have been reported of various nano-phases confined in slit-shaped pores composed of parallel 2D sheets; it has been shown that the confined molecules are subject to very high pressures [46,47]. Vasu et al. [12] studied triphenylamine and boric acid confined in a slit pore composed of two graphene sheets, with a pore width of 1 nm. The structure of these molecules is pressure sensitive, and these researchers used Raman spectroscopy to determine the structure of the molecules in the graphene pore. By comparing the observed molecular structure with structure results from Raman studies on the bulk materials, they were able to estimate an effective pressure of 1.2 GPa in the pore. This finding agrees quite well with molecular simulation results that we have obtained for slit carbon pores [20,25]. Similar high effective pressures, in the range 1–10 GPa, have been observed recently in other similar experiments by this research group and others [11,13,14,46,47]. Although these experiments confirm the strong pressure enhancement that occurs in carbon pores, the pressures reported are not well-defined, since the "effective bulk pressure" is a scalar, whereas the actual pressure in the pores is a second-order tensor.

4.3. High-pressure reactions in nano-pores

Chemical reactions that require a high pressure when carried out in the bulk phase are often found to give a high yield of product when carried out in a nano-porous material, even though the bulk phase in equilibrium with the pore phase is at low pressure. We give two examples here.

4.3.1. Nitric oxide dimerization reaction

In 1989, Kaneko et al. [48] reported a study of the nitric oxide (NO) dimer reaction, $2NO = (NO)_2$, in activated carbon fibers (pore width of 0.8–0.9 nm) with slit-shaped pores for temperatures ranging from 273 to 423 K. Magnetic susceptibility measurements showed that the reaction went almost to completion in the nanopores (more than 98 mol% dimers), even though the proportion of dimers in the bulk phase in equilibrium with the pore was of the order of a few mole percent or less. This surprising result was confirmed in later experiments carried out by Byl et al. [49], who studied the reaction in (10,10) SWCNTs (diameter of 1.36 nm) over the temperature range 103–136 K. Equilibrium compositions within the SWCNTs were determined using Fourier-transform infrared (FTIR) spectroscopy, and the mole percent of the dimers was shown to be 100% within the experimental error, which was estimated to be 5%. Subsequent theoretical and molecular simulation (reactive Monte Carlo) studies by various groups [50–52] failed to reproduce the experimental results. The predicted yield of the dimer, while higher than in the bulk phase, was considerably lower than that found in the experiments. Also, the yield was predicted to decrease rapidly with increasing temperature, whereas the experiments showed no discernible effect of temperature on the yield. Recently, Srivastava et al. [53] showed that the failure of the earlier theoretical predictions was due to the neglect of strong association interactions between the dimers and the π electrons in the carbon walls. *Ab initio* calculations at the MP2 (short for second-order Møller–Plesset perturbation theory) level showed that the interaction energy between the $(NO)_2$ dimer molecule and the carbon wall was nearly 20 times stronger than that expected from van der Waals forces, as assumed in the previous studies. When this was accounted for in the molecular simulations, good agreement with the experiments for both the yield and its temperature dependence was obtained for both activated carbon fibers and carbon nanotubes. The tangential pressure in the *z* direction (parallel to the pore walls) was calculated to be of the order of several hundred thousand bars near the pore walls, due to the strong attractive forces with the pore wall.

4.3.2. Reactions in aqueous solutions

Vasu et al. [12] studied the effect of confinement in graphene slit pores on aqueous solutions of several salts: magnesium chloride ($MgCl_2$), cesium iodide (CsI), copper(II) sulfate ($CuSO_4$), and calcium hydroxide ($Ca(OH)_2$). They found that these compounds, which are unreactive with water under bulk-phase conditions at room pressure, react with water in the confined nano-phase to yield the corresponding metal oxide (with the exception of CsI, which does not react), due to the high pressure in the nano-pores. They confirmed the conversion to the oxide using energy-dispersive X-ray (EDX) spectroscopy, electron diffraction, and electron energy-loss spectroscopy (EELS). These experiments unequivocally showed that the observed crystals in the pores are the oxide.

It is known from high-pressure experiments on bulk aqueous solutions [54] that increasing the pressure from 0.1 MPa (1 bar) to 1 GPa (10 000 bar) causes the ionization constant of water to increase by two orders of magnitude, thus favoring hydrolysis of the salts. It is proposed that the confinement-induced high pressure causes the salts to hydrolyze to their hydroxides followed by decomposition to the corresponding oxides. In the bulk phase, conversion of these salts to their hydroxides or oxides was only observed previously at high temperatures and pressures [55]. Therefore, the nano-confinement and resulting high pressure is accepted to be sufficient to cause the reaction to occur at room temperature. They also studied $MgCl_2$ dissolved in methanol in these graphene pores and observed no reaction; this finding was expected since there is no ionization of the solvent. Other recent experimental observations of the high reactivity of water in nano-confinement have been reported by Lim et al. [46,47].

4.4. New high-pressure materials synthesis in confinement: The insulator–metal transition

Fujimori et al. [56] reported the formation of a 1D metallic sulfur (S) phase when the sulfur is confined within SWCNTs or double-walled carbon nanotubes (DWCNTs) with a diameter of about 1 nm and is in equilibrium with a bulk sulfur vapor phase at sub-ambient pressure (Fig. 4(a)). The confined sulfur forms either a linear or a zigzag covalently bonded chain, depending on the precise diameter of the nanotube, as confirmed by HRTEM and synchrotron XRD. The chains have long domain sizes (up to 160 nm) and are thermally stable at temperatures up to about 800 K. The S–S bond lengths for the linear chains are about 0.19 nm, which is shorter than the bond length of bulk-phase polymeric sulfur, S_Ψ, which has a bond length of about 0.207 nm, suggesting strong chemical bonding. The reduced bond length and the metallic nature of the 1D phase suggest that the sulfur chain is under a strong tangential pressure in the pore. This behavior of confined sulfur is in strong contrast with that of bulk sulfur, for which 1D chains are unstable, and for which a 3D metallic phase only appears at pressures of the order of 95 GPa. Molecular dynamics (MD) simulations performed recently by our group [27] predict that the tangential pressure in the center of the sulfur chain is of the order of 700 GPa, which is well above the bulk-phase pressure at which metallic sulfur forms.

Fujimori et al. [57] also observed the formation of a double-helix structure of covalently bonded selenium (Se) (Fig. 4(b)) in DWCNTs with a diameter of about 1 nm, as confirmed by HRTEM, XRD, and *ab initio* calculations. The confined Se double helices are radially compressed in the pores. This is a new structural phase of Se that is quite different from the structures seen in bulk Se.

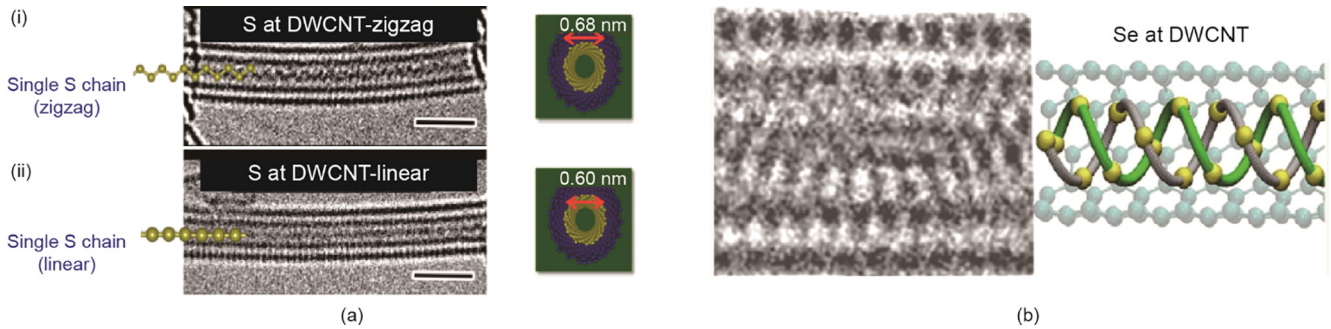

Fig. 4. (a) HRTEM images of sulfur (S) confined within carbon nanotubes: (i) Zigzag chain inside a DWCNT of 0.68 nm diameter; (ii) 1D linear sulfur chain inside a DWCNT of 0.60 nm diameter [56]. The scale bar is 1 nm. (b) Double-helix structure of selenium (Se) confined in a DWCNT with a diameter of about 1 nm [57]. (Adapted from Refs. [56,57])

Recently, the formation of a 1D tellurium chain encapsulated in SWCNTs with diameters between 0.7 and 1.1 nm has been reported by Medeiros et al. [58]. The transition from metallic to insulating behavior was observed as the nanotube diameter was increased. Nano-confinement is not only a means to produce this novel phase, but is also necessary to ensure the mechanical stability of the confined species.

5. Theory and molecular simulation studies of surface-driven high pressures

Quite extensive molecular simulation studies have been done of both the normal and tangential pressures for adsorbed films in nano-pores of simple geometries for non-reactive systems that interact with simple van der Waals forces. For cases where chemical reaction occurs, either between the molecules in the adsorbed film or between those molecules and the pore walls, much less work has been done and the pressures in such systems are not well understood at present.

5.1. Non-reacting systems with simple van der Waals forces

Starting in 2011, a number of studies have used semi-grand canonical Monte Carlo (SGMC) simulations to calculate the pressure tensor components for a simple nonpolar fluid in nanoporous carbons and silicas with slit, cylindrical, and spherical-shaped pores [20–22,24–28]. These studies have demonstrated that the normal and tangential pressure components are usually very large—up to thousands of bars for the normal pressure and tens of thousands of bars for the tangential pressure. These pressures are in qualitative agreement with the experimental observations to date. In the simulations, the pores are of finite length and are in direct contact with the bulk gas phase, thus ensuring that the condition of mechanical (or hydrostatic) equilibrium (i.e., no net momentum transfer at equilibrium), Eq. (3), is obeyed.

Typical results for carbon pores with a width of 15 molecular diameters (about 5 nm) at 87.3 K and 1 bar bulk pressure (the boiling point of argon) and adsorbate molecules that exhibit simple van der Waals (LJ) interactions are shown in Fig. 5(a). The tangential pressure in the contact layer next to the pore wall is about 19 000 bar, while in the center of the pore it is oscillating about ±200 bar (see inset in Fig. 5(a), which shows the pressure on an expanded scale). For smaller pores, P_T is considerably higher—as high as 60 000 bar for small slit-shaped nano-pores with a width of 2 molecular diameters at temperatures in the liquid range [20,25]. These very large positive tangential pressures arise from the strongly repulsive intermolecular forces between neighboring molecules in the *xy* plane (Fig. 1). The normal pressure, P_N, for this system is shown as the black horizontal line, and is constant across the pore at about 27 bar. Fig. 5(b) shows the normal pressure versus the pore width for carbon tetrachloride (CCl_4) confined with slit pores (a model of activated carbon fibers) from both experiment and simulation. The experimental values were obtained by observing the change in the interlayer spacing of the graphene layers using XRD data, together with the estimated Young's modulus. The normal pressure can be either positive or negative, depending on the pore width. This oscillating behavior with increasing pore width is known from a variety of experimental studies, and is due to packing effects in the pore.

An examination of the statistical mechanical equations for the pressure shows that the pressure depends on the temperature, the pressure of the bulk phase, and the wetting characteristics of the adsorbed molecules on the solid surface. A quantitative measure of the wetting is provided by the microscopic wetting parameter [20], α_w, the ratio of fluid–wall interactions to fluid–fluid interactions, as given by the following equation:

$$\alpha_w = \frac{\text{Fluid–wall interaction}}{\text{Fluid–fluid interaction}} = \rho_s \sigma_{fw}^2 \Delta \left(\frac{\varepsilon_{fw}}{\varepsilon_{ff}}\right) \quad (7)$$

where ρ_s and Δ are the number density of the solid atoms and the spacing between atomic layers in the solid (ρ_s = 114 nm^{-3} and Δ = 0.335 nm for graphite), and ε and σ are the usual LJ parameters for the fluid–fluid (adsorbate–adsorbate) (ff) and fluid–wall (fw) interactions. The molecular simulation studies show that the tangential pressure increases rapidly with increase in the wetting parameter (Fig. 3). It also increases very rapidly (roughly exponentially) with increase in the pressure of the bulk phase in equilibrium with the pore phase.

5.2. Confined systems in which chemisorption or chemical reaction occurs

Although little work has been reported on surface-driven high pressures in thin adsorbed films when chemisorption or chemical reaction occurs, it appears that even higher tangential pressures can occur, at least in some cases. Recently, Srivastava et al. [28] reported a systematic study of the effect of surface wetting, pore width, and adsorbate molecular shape on the pressure tensor components P_N and P_T for slit-shaped pores. Included in this study were molecules that are weakly chemisorbed by the pore walls. Values of α_w up to 40 were studied, corresponding to the chemisorption of the nitric oxide dimer, $(NO)_2$, with the carbon wall. Tangential pressures near the pore walls ranged from 100 000 to 500 000 bar for these stronger interactions.

Recently, MD simulations [27] were reported for sulfur in a carbon nanotube (CNT) of the same diameter and chirality as that

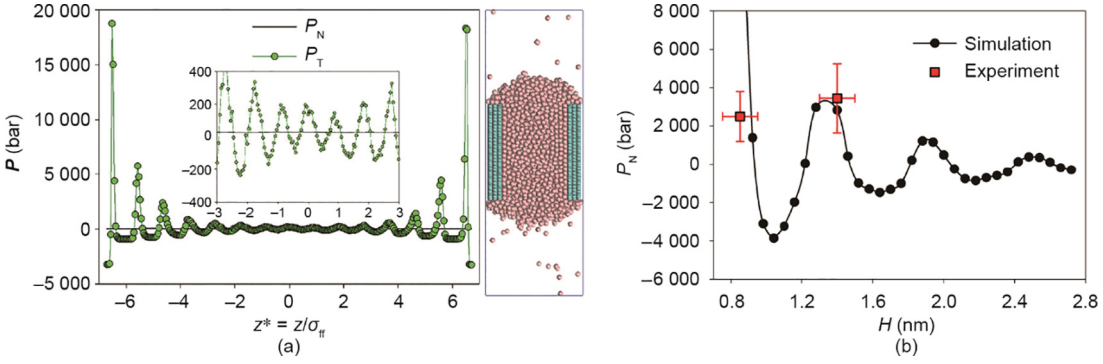

Fig. 5. (a) (Left) Normal and tangential pressures for Ar at its normal boiling point in a slit-shaped carbon pore with a width of $H = 15\sigma_{Ar}$ [25]; (right) a snapshot of the simulation of the nano-pore phase in equilibrium with the gas phase. (b) Normal pressure versus pore width (H) for CCl_4 adsorbed in activated carbon fibers at 300 K [21]. (Adapted from Refs. [21,25])

used in the experiments of Fujimori et al. [56] (see Fig. 4(a) and associated discussion). A modified form of the reactive force field of Stillinger and Weber (SW) [59] was used for the sulfur interactions. Results for the structure and tangential pressure of the confined sulfur nano-phase are shown in Fig. 6(a) and (b). The sulfur atoms, which are strongly covalently bonded, have a bond length of 0.189 nm, which is in good agreement with the experimental value of (0.18 ± 0.02) nm [27], but is substantially smaller than the bond length of polymeric sulfur, S_Ψ, (0.207 nm) in the bulk phase. The peak local tangential pressure is of the order of 700 GPa. Such a high pressure is quite sufficient to lead to a metallic phase, as observed in the experiments (the insulator–metal transition occurs at about 95 GPa for bulk sulfur). These calculations are qualitative in nature, since the force field used was fitted to the bulk-phase dimer properties. However, there is experimental evidence that the bond strength in the confined nano-phase is close to that for the bulk dimer [27]. In the MD simulations, varying the force field energy by 10%–20% caused the calculated tangential pressure to change, although it remained within the range from 4 to 10 GPa, which is sufficient to explain the metallic behavior of the sulfur chain.

An analysis of the forces and potential energies experienced by the sulfur atoms in the pore indicates that the interaction with the pore walls is strongly repulsive (Fig. 6(c)). However, the sulfur–sulfur interactions are so strongly attractive, due to chemical bonding, that the sulfur chain can lower its free energy by entering the pore and is strongly stabilized by the carbon nano-pores. Examination of the contributions to the tangential pressure shows that it is this repulsive interaction with the pore walls, enabled by the strong sulfur–sulfur bonding, that produces the very high pressures.

6. Conclusions

Pressure is a fundamental thermodynamic variable that has the potential to control and enhance the manufacture of chemicals and solid materials with a wide range of desired properties. Existing industrial processes achieve high pressures through mechanical compression, typically of a bulk gas mixture, and are exemplified by the production of ammonia from hydrogen and nitrogen gases, as demonstrated by Fritz Haber in 1909, using pressures of around 20 MPa. However, such high-pressure processes are limited in application because of cost and difficulties in compressor design (i.e., materials considerations). The development of surface-driven high-pressure chemical reactions, chemical processing, and materials synthesis would offer great benefits and could transform the use of pressure as a decisive variable in industrial manufacturing. Since high pressure is provided by the attractive force field from the surface of the substrate, this would obviate the high cost and materials difficulties of conventional compression. More importantly, such surface-driven high-pressure processes would provide a simple means of achieving much higher pressures—up to tens of thousands of bars and higher in some operations—than are currently accessible at the industrial scale. In addition, since the principal pressure component is the tangential pressure acting parallel to the solid surface, such processes would avoid the problem of very high pressures acting on the walls of the reactor vessel, and thus avoid the failure of materials.

On first consideration, one might think of several possible objections to the practical application of these surface-driven high-pressure effects. For example:

(1) Since the high-pressure region only extends a few nanometers from the substrate surface, the active processing zone will be too small. However, a simple calculation shows that this is not the case in general, mainly because activated carbons have a very large surface area—typically 1000–2000 $m^2 \cdot g^{-1}$. Such carbons have a density of about 0.5 $g \cdot cm^{-3}$ and micropore widths of 1–2 nm. Assuming a surface area of 1000 $m^2 \cdot g^{-1}$ and a mean pore width of 2 nm (the active processing zone), an adsorption column with a diameter of 2 m and a height of 10 m would contain about 15 000 kg of carbon and have an active processing zone of 30 m^3.

(2) When removed from the active processing zone, the pressure is low and the product will revert to its original low-pressure form. This would happen in some cases in which the transition barrier is low and the product is not in the equilibrium phase

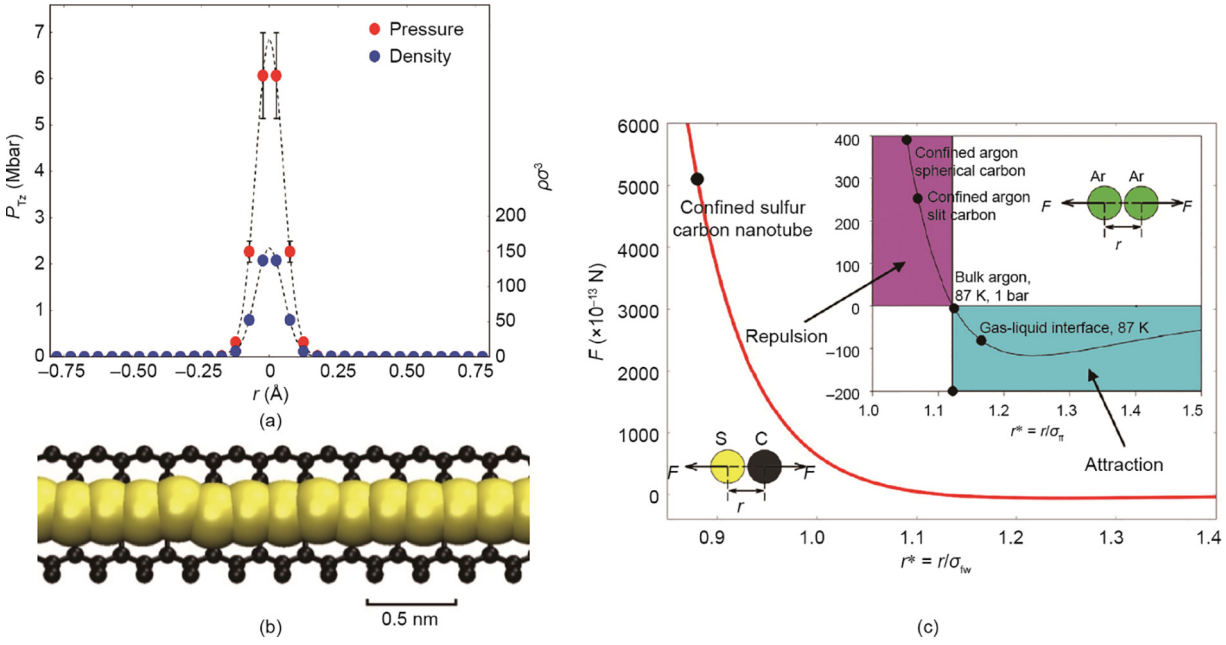

Fig. 6. (a) Tangential pressure and number density for sulfur atoms and (b) 1D sulfur phase in an (8,0) SWCNT with a diameter of 0.626 nm, from MD simulation [27]. (c) Analysis of the forces and potential energies experienced by the sulfur atoms in the pore: Red curve indicates the intermolecular force between a sulfur atom (S) and a carbon wall atom (C) for sulfur in the (8,0) SWCNT; the force for the average S–C separation distance is shown by the black circle. Inset is the corresponding Ar/Ar force curve for LJ Ar atoms next to a carbon wall in slit-shaped and spherical carbon pores [27]. (Adapted from Ref. [27])

under low-pressure conditions. However, there will be many cases in which this will not happen, either because the final product is the true thermodynamic equilibrium state, or because the final product is metastable but does not revert to the true equilibrium form because of a high activation barrier (for example, diamond under ambient conditions). At the laboratory scale, for example, many chemical reactions are kinetically limited due to a high activation-energy barrier, and high pressure, often ranging from 0.1 to 3 GPa, is needed to overcome this.

(3) It is difficult to remove the product from the narrow pores. This may be the case for some applications, such as the nanowires of sulfur and tellurium that are formed within narrow carbon nanotubes. However, it is likely that there are many applications where removal of the product is possible, such as by solvent extraction, sonication, lowering the bulk-phase pressure, or other methods.

7. Outlook

In order to achieve surface-driven high-pressure processing in practice, it will first be necessary to build a sufficient fundamental knowledge base, including the best ways to produce, control, and measure such surface-driven high pressures. Reliable methods for the theoretical modeling of these processes will require the development and testing of approaches at the electronic, atomistic, and mesoscales of matter in order to account for confinement and strong compression, and to determine reaction mechanisms, activated states and barriers, reaction rates, and diffusion rates, all in confinement. Basic research is also needed to develop experimental methods to more precisely control and characterize surface geometry, chemistry, pore size, and pore shape in the synthesis of nano-porous materials, and to investigate and control the entry of reactant molecules into the pores and the products out of the pores.

This field is in its infancy; however, many areas are ripe for future investigation. Examples include the following:

(1) Studies of prototype chemical reactions that require high pressure. In some cases, surface-driven high pressure may favor the reaction due to equilibrium thermodynamics, for example because the number of moles is decreased as a result of the reaction (Le Chatelier's principle). In these cases, experimental studies of the reaction yield should be coupled with molecular simulations to calculate the equilibrium yield (reactive Monte Carlo) and free energies (e.g., through histogram reweighting or density-of-states methods [60]) involved. In the case of reactions that are kinetically limited due to high activation barriers, it will be of interest to study how high the pressure must be to overcome the barrier, and how the reaction can be controlled by manipulation of the adsorbent material, pore size, and shape. Can we make use of the surface properties of the solid substrate to select the best reaction pathway and final product? Again, it will be highly desirable to combine experimental investigations with theory (e.g., density functional theory and string optimization methods to determine the reaction path and activated state).

(2) Reactions in aqueous solution. High-pressure experiments on water and aqueous solution in the bulk phase have shown that the ionization constant of water is increased by orders of magnitude [54], and that this leads to greatly increased reactivity [55]. Recently, several works have been reported [12,46,47] in which hydrolysis reactions are observed in salt solutions confined within graphene nanobubbles, apparently due to surface-driven compression. This is a rich area for further investigation.

(3) The effect of surface-driven high pressure on phase changes. Much work has been done on gas–liquid condensation and melting/freezing for pure substances in nano-pores and on solid substrates. However, industrial processes such as distillation, gas adsorption, liquid–liquid extraction, membrane separation, crystallization, and supercritical extraction usually involve mixtures, and very little is known about the surface-compression effects of mixtures. Areas in which little or no work has yet been done include the effects of surface-driven compression and confinement on the solubility of dilute solutes in liquid solvents [61], on the fluid and solid regions of the phase diagrams for the six known classes of binary mixtures [30,61–64], and on high-pressure solid–solid transitions [62,64].

(4) Exploring the conditions needed to produce desired polymorphs (including new polymorphs) of pharmaceuticals and other specialty chemicals. These conditions might include the type of adsorbent substrate, surface conditions, and pore size and shape.

(5) The effect of very high pressures on the electronic and photonic properties of materials [1]. Of particular interest are the changes to electronic bandwidths and bandgaps induced by high pressure, and the resulting insulator–metal, insulator–semiconductor, and semiconductor–metal transitions, as well as the transitions to magnetic and superconducting states [1,65–69]. Much work has been done on these transitions for bulk elements and compounds, using shock compression or anvil cell measurements. In bulk materials, these transitions occur at pressures ranging from below 1 to 200 GPa or more. Recent work has shown that confinement in SWCNTs of suitable diameter is sufficient to cause an insulator–metal transition for both sulfur [56] and tellurium [58] (both of which are group VIB elements in the periodic table), and theoretical calculations [27] suggest that this is a surface-driven high-pressure effect with tangential pressures of several hundred gigapascals (Fig. 6).

(6) The effect of surface-driven high pressures on atomic and molecular properties—molecular configuration, vibrational modes, bond angles, and so forth. Methods for such studies might include FTIR and Raman spectroscopy [12].

(7) The development of experimental techniques to measure the compression of adsorbed nano-phases near solid substrates and the local properties of these phases, including the effective tangential pressures near the surface of the substrate. It may be possible to estimate the latter for adsorbed monolayers on a flat surface by using small-angle neutron diffraction to determine the local density, together with a theoretical EOS to determine the tangential pressure (see Fig. 3 and associated discussion, where the effective tangential pressure is estimated from molecular simulation results for the number density in the compressed adsorbed monolayer). FTIR and Raman spectroscopy offer one possible route to observe the effect of compression near surfaces on individual molecules.

Acknowledgments

The authors would like to thank several colleagues for helpful discussions and cooperation on the topic of pressure enhancement in thin adsorbed films, including Cody Addington, Katsumi Kaneko, Jeremy Palmer, and Fanxing Li. We also thank two anonymous referees for helpful comments and suggestions. We are grateful to the US National Science Foundation (CBET-1603851 and CHE-1710102) for support of this work. Małgorzata Śliwińska-Bartkowiak thanks the National Science Center of Poland (DEC-2013/09/B/ST4/03711) for support.

Compliance with ethics guidelines

Keith E. Gubbins, Kai Gu, Liangliang Huang, Yun Long, J. Matthew Mansell, Erik E. Santiso, Kaihang Shi, Małgorzata Śliwińska-Bartkowiak, and Deepti Srivastava declare that they have no conflict of interest or financial conflicts to disclose.

References

[1] Zhang L, Wang Y, Lv J, Ma Y. Materials discovery at high pressures. Nat Rev Mater 2017;2(4):17005.
[2] Gregg SJ, Sing KSW. Adsorption surface area and porosity. London: Academic Press; 1967.
[3] Gregg SJ, Sing KSW. Adsorption, surface area and porosity. 2nd ed. London: Academic Press; 1982.
[4] Karnaukhov AP. Improvement of methods for surface-area determinations. J Colloid Interface Sci 1985;103(2):311–20.
[5] Aranovich GL, Donohue MD. Surface compression in adsorption systems. Colloids Surf 2001;187–188:95–108.
[6] Chu YS, Robinson IK, Gewirth AA. Properties of an electrochemically deposited Pb monolayer on Cu(111). Phys Rev B 1997;55(12):7945–54.
[7] Schabes-Retchkiman S, Venables JA. Structural studies of xenon and krypton solid monolayers on graphite using transmission electron diffraction. Surf Sci 1981;105(2–3):536–64.
[8] Calisti S, Suzanne J, Venables JA. A LEED study of adsorbed neon on graphite. Surf Sci 1982;115(3):455–68.
[9] Van Bavel AP, Hopstaken MJP, Curulla D, Niemantsverdriet JW, Lukkien JJ, Hilbers PAJ. Quantification of lateral repulsion between coadsorbed Co and N on Rh(100) using temperature-programmed desorption, low-energy electron diffraction, and Monte Carlo simulations. J Chem Phys 2003;119(1):524–32.
[10] Al-Sarraf N, King DA. Calorimetric adsorption heats on low-index nickel surfaces. Surf Sci 1994;307–309(Pt A):1–7.
[11] Ghorbanfekr-Kalashami H, Vasu KS, Nair RR, Peeters FM, Neek-Amal M. Dependence of the shape of graphene nanobubbles on trapped substance. Nat Commun 2017;8:15844.
[12] Vasu KS, Prestat E, Abraham J, Dix J, Kashtiban RJ, Beheshtian J, et al. Van der Waals pressure and its effect on trapped interlayer molecules. Nat Commun 2016;7:12168.
[13] Khestanova E, Guinea F, Fumagalli L, Geim AK, Grigorieva IV. Universal shape and pressure inside bubbles appearing in van der Waals heterostructures. Nat Commun 2016;7:12587.
[14] Zamborlini G, Imam M, Patera LL, Menteş TO, Stojić N, Africh C, et al. Nanobubbles at GPa pressure under graphene. Nano Lett 2015;15(9):6162–9.
[15] Parsonage NG. Monte Carlo studies of a two-dimensional commensurate-incommensurate system—effects of change of particle size and interaction parameters at constant number density. J Chem Soc Faraday Trans 1992;88(6):777–87.
[16] Rittner F, Boddenberg B, Bojan MJ, Steele WA. Adsorption of nitrogen on rutile (110): Monte Carlo computer simulations. Langmuir 1999;15(4):1456–62.
[17] Nguyen VT, Do DD, Nicholson D. On the heat of adsorption at layering transitions in adsorption of noble gases and nitrogen on graphite. J Phys Chem C 2010;114(50):22171–80.
[18] Aranovich GL, Donohue MD. Adsorption compression: an important new aspect of adsorption behavior and capillarity. Langmuir 2003;19(7):2722–35.
[19] Wetzel TE, Erickson JS, Donohue PS, Charniak CL, Aranovich GL, Donohue MD. Monte Carlo simulations on the effect of substrate geometry on adsorption and compression. J Chem Phys 2004;120(24):11765–74.
[20] Long Y, Palmer JC, Coasne B, Śliwinska-Bartkowiak M, Gubbins KE. Pressure enhancement in carbon nanopores: a major confinement effect. Phys Chem Chem Phys 2011;13(38):17163–70.
[21] Śliwińska-Bartkowiak M, Drozdowski H, Kempiński M, Jażdżewska M, Long Y, Palmer JC, et al. Structural analysis of water and carbon tetrachloride adsorbed in activated carbon fibres. Phys Chem Chem Phys 2012;14(19):7145–53.
[22] Long Y, Palmer JC, Coasne B, Śliwinska-Bartkowiak M, Gubbins KE. Under pressure: quasi-high pressure effects in nanopores. Microporous Mesoporous Mater 2012;154(19):19–23.
[23] Abaza S, Aranovich GL, Donohue MD. Adsorption compression in surface layers. Mol Phys 2012;110(11–12):1289–98.
[24] Long Y, Śliwinska-Bartkowiak M, Drozdowski H, Kempinski M, Phillips KA, Palmer JC, et al. High pressure effect in nanoporous carbon materials: effects of pore geometry. Colloids Surf A 2013;437:33–41.
[25] Long Y, Palmer JC, Coasne B, Śliwinska-Bartkowiak M, Jackson G, Müller EA, et al. On the molecular origin of high-pressure effects in nanoconfinement: the role of surface chemistry and roughness. J Chem Phys 2013;139(14):144701.
[26] Coasne B, Long Y, Gubbins KE. Pressure effects in confined nanophases. Mol Simul 2014;40(7–9):721–30.
[27] Addington CK, Mansell JM, Gubbins KE. Computer simulation of conductive linear sulfur chains confined in carbon nanotubes. Mol Simul 2017;43(7):519–25.
[28] Srivastava D, Santiso EE, Gubbins KE. Pressure enhancement in confined fluids: effect of molecular shape and fluid-wall interactions. Langmuir 2017;33(42):11231–45.
[29] Schofield P, Henderson JR. Statistical mechanics of inhomogeneous fluids. Proc R Soc A 1982;379(1776):231–46.
[30] Gray CG, Gubbins KE, Joslin CG. Theory of molecular fluids. 2. Applications. Oxford: Oxford University Press; 2011.
[31] Addington CK, Long Y, Gubbins KE. The pressure in interfaces having cylindrical geometry. J Chem Phys 2018. In press.
[32] Irving JH, Kirkwood JG. The statistical mechanical theory of transport processes. IV. The equations of hydrodynamics. J Chem Phys 1950;18(6):817–29.
[33] Shi K, Gu K, Shen Y, Srivastava D, Santiso EE, Gubbins KE. High density equation of state for a two-dimensional Lennard-Jones solid. J Chem Phys 2018;148(17):174505.
[34] Günther G, Prass J, Paris O, Schoen M. Novel insights into nanopore deformation caused by capillary condensation. Phys Rev Lett 2008;101(8):086104.
[35] Urita K, Shiga Y, Fujimori T, Iiyama T, Hattori Y, Kanoh H, et al. Confinement in carbon nanospace-induced production of KI nanocrystals of high-pressure phase. J Am Chem Soc 2011;133(27):10344–7.
[36] Cui ST, McCabe C, Cummings PT, Cochran HD. Molecular dynamics study of the nano-rheology of *n*-dodecane confined between planar surfaces. J Chem Phys 2003;118(19):8941–4.
[37] Kumacheva E, Klein J. Simple liquids confined to molecularly thin layers. II. Shear and frictional behavior of solidified films. J Chem Phys 1998;108(16):7010–22.
[38] Klein J, Kumacheva E. Simple liquids confined to molecularly thin layers. I. Confinement-induced liquid-to-solid phase transitions. J Chem Phys 1998;108(16):6996–7009.
[39] Klein J, Kumacheva E. Confinement-induced phase transitions in simple liquids. Science 1995;269(5225):816–9.
[40] Hu HW, Carson GA, Granick S. Relaxation time of confined liquids under shear. Phys Rev Lett 1991;66(21):2758–61.
[41] Fujiwara Y, Nishikawa K, Iijima T, Kaneko K. Simulation of small-angle X-ray scattering behavior of activated carbon fibers adsorbing water. J Chem Soc Faraday Trans 1991;87(17):2763–8.
[42] Asaumi K, Mori T. High-pressure optical absorption and X-ray-diffraction studies in RbI and KI approaching the metallization transition. Phys Rev B 1983;28(6):3529–33.
[43] Casco ME, Silvestre-Albero J, Ramírez-Cuesta AJ, Rey F, Jordá JL, Bansode A, et al. Methane hydrate formation in confined nanospace can surpass nature. Nat Commun 2015;6(1):6432.
[44] Fu Q, Bao X. Surface chemistry and catalysis confined under two-dimensional materials. Chem Soc Rev 2017;46(7):1842–74.
[45] Novoselov KS, Mishchenko A, Carvalho A, Castro Neto AH. 2D materials and van der Waals heterostructures. Science 2016;353(6298):aac9439.
[46] Lim CH, Nesladek M, Loh KP. Observing high-pressure chemistry in graphene bubbles. Angew Chem Int Ed 2014;53(1):215–9.
[47] Lim CH, Sorkin A, Bao Q, Li A, Zhang K, Nesladek M, et al. A hydrothermal anvil made of graphene nanobubbles on diamond. Nat Commun 2013;4:1556.
[48] Kaneko K, Fukuzaki N, Kakei K, Suzuki T, Ozeki S. Enhancement of NO dimerization by micropore fields of activated carbon-fibers. Langmuir 1989;5(4):960–5.
[49] Byl O, Kondratyuk P, Yates JT. Adsorption and dimerization of NO inside single-walled carbon nanotubes—an infrared spectroscopic study. J Phys Chem B 2003;107(18):4277–9.
[50] Lísal M, Brennan JK, Smith WR. Chemical reaction equilibrium in nanoporous materials: NO dimerization reaction in carbon slit nanopores. J Chem Phys 2006;124(6):064712.
[51] Tripathi S, Chapman WG. A density functional approach to chemical reaction equilibria in confined systems: application to dimerization. J Chem Phys 2003;118(17):7993–8003.
[52] Turner CH, Johnson JK, Gubbins KE. Effect of confinement on chemical reaction equilibria: the reactions $2NO \Leftrightarrow (NO)_2$ and $N_2 + 3H_2 \Leftrightarrow 2NH_3$ in carbon micropores. J Chem Phys 2001;114(4):1851–9.
[53] Srivastava D, Turner CH, Santiso EE, Gubbins KE. The nitric oxide dimer reaction in carbon nano-pores. J Phys Chem B 2018;122(13):3604–14.
[54] Marshall WL, Franck EU. Ion product of water substance, 0–1000 °C, 1–10 000 bars new international formulation and its background. J Phys Chem Ref Data 1981;10(2):295–304.
[55] Ding Y, Zhang GT, Wu H, Hai B, Wang LB, Qian YT. Nanoscale magnesium hydroxide and magnesium oxide powders: control over size, shape, and structure via hydrothermal synthesis. Chem Mater 2001;13(2):435–40.
[56] Fujimori T, Morelos-Gómez A, Zhu Z, Muramatsu H, Futamura R, Urita K, et al. Conducting linear chains of sulphur inside carbon nanotubes. Nat Commun 2013;4:2162.
[57] Fujimori T, dos Santos RB, Hayashi T, Endo M, Kaneko K, Tománek D. Formation and properties of selenium double-helices inside double-wall carbon nanotubes: experiment and theory. ACS Nano 2013;7(6):5607–13.
[58] Medeiros PVC, Marks S, Wynn JM, Vasylenko A, Ramasse QM, Quigley D, et al. Single-atom scale structural selectivity in Te nanowires encapsulated inside ultra-narrow, single-walled carbon nanotubes. ACS Nano 2017;11(6):6178–85.
[59] Stillinger FH, Weber TA. Molecular dynamics study of chemical reactivity in liquid sulfur. J Phys Chem 1987;91(19):4899–907.
[60] Chipot C, Pohorille A. Free energy calculations. Berlin: Springer; 2007.
[61] Hu Y, Huang L, Zhao S, Liu H, Gubbins KE. Effect of confinement in nano-porous materials on the solubility of a supercritical gas. Mol Phys 2016;114(22):3294–306.
[62] Streett WB. Gas-gas equilibrium: high pressure limits. Can J Chem Eng 1974;52(1):92–7.
[63] Schneider GM. High pressure thermodynamics of mixtures. Pure Appl Chem 1976;47(4):277–91.

[64] Rowlinson JS, Swinton FL. Liquids and liquid mixtures. 3rd ed. London: Butterworth Scientific Press; 1982.
[65] Schneider GM. High pressure investigations on fluid systems—a challenge to experiment, theory, and application. J Chem Thermodyn 1991;23(4):301–26.
[66] Minomura S. Pressure-induced insulator-metal transition. In: Fritzshe H, Adler D, editors. Localization and metal-insulator transitions. New York: Plenum Press; 1985. p. 63–76.
[67] Chacham H, Zhu X, Louie SG. Pressure-induced insulator-metal transitions in solid xenon and hydrogen: a first-principles quasiparticle study. Phys Rev B 1992;46(11):6688–99; Erratum in: Phys Rev B 1993;48(3):2025.
[68] Hemley RJ, Ashcroft NW. The revealing role of pressure in the condensed matter sciences. Phys Today 1998;51(8):26–32.
[69] Imada M, Fujimori A, Tokura Y. Metal-insulator transitions. Rev Mod Phys 1998;70(4):1039–263.